Draft version February 22, 2016
Preprint typeset using LaTeX style emulateapj v. 08/22/09

A DICHOTOMY IN THE RELATIVE VELOCITY OF LYα ABSORPTION IN NEARBY GALAXY HALOS

David M. French, Bart P. Wakker
Department of Astronomy, University of Wisconsin - Madison
Draft version February 22, 2016

ABSTRACT

We present initial results from an ongoing large-scale study of the circumgalactic medium in the nearby Universe ($cz \leq 10,000$ km/s), using archival Cosmic Origins Spectrograph (COS) and Space Telescope Imaging Spectrograph (STIS) spectra of background QSOs. This initial sample contains 35 sight lines, yielding 175 Lyα systems, 56 of which we have paired with nearby galaxies. We introduce a likelihood parameter to quantitatively predict the galaxy responsible for measured absorption in a reproducible way. We find a dichotomy in the equivalent widths (W) of absorption systems around $\Delta v = v_{galaxy} - v_{gas}$, with positive Δv absorption $W = 380 \pm 14$ mÅ, and negative Δv absorption $W = 163 \pm 15$ mÅ. This W difference is significant at a greater than 99% confidence limit. We also find a preference for absorption around highly inclined galaxies, but little evidence of azimuthal dependence.

Subject headings: IGM, CGM, galaxies

1. INTRODUCTION

It is well known that galaxies must continue to accrete gas throughout their lifetimes in order to sustain observed levels of star formation (e.g. Erb 2008, Putman et al. 2009b). This additional gas must come from the diffuse intergalactic medium (IGM), where the majority of the baryons in the universe reside (CITATION?). How exactly this IGM gas eventually falls into the halos and disks of galaxies is still highly uncertain, as observational constraints are hard to come by. Because of the diffuse nature of IGM gas, it is most readily and sensitively detected as absorption in the spectra of background active galactic nuclei (AGN). The advent of the sensitive UV spectrographs STIS and COS on the Hubble Space Telescope (HST) has provided a wealth of information on the properties and distribution of both the ions of heavy elements as well as the Lyman series of neutral H I gas around galaxies.

Individual concentrations of gas along a given sightline imprint absorption lines on the spectrum in the direction of the QSO. The metal lines trace the star formation history within the intervening gas, and neutral hydrogen lines (Lyα) indicate both the location and velocities of outflowing gas as well as the presence of fuel for future star formation. Numerous studies using these observations have shown that many Lyα absorbers trace individual galaxy halos (e.g. Wakker & Savage 2009, Danforth et al. 2014, Stocke et al. 2013 & 2014, Liang et al 2014, Lanzetta et al 1995, Chen et al. 1998, 2001a, Tripp et al. 1998, Steidel et al. 2010, Prochaska et al. 2011, Thom et al 2012, Tumlinson et al. 2011 & 2013).

Some recent studies find that about half of Lyα absorbers lie within galaxy haloes, at impact parameters $\rho < 350$ kpc (Côté et al. 2005, Prochaska et al. 2006). In addition, Wakker & Savage (2009) find that for 90% of L$> 0.1L_*$ galaxies an absorber lies within 400 kpc and 400 km/s, and all galaxies have a Lyα absorber within 1.5 Mpc. Higher redshift studies, such as Rudie et al. (2012) at $2 < z < 3$, find evidence for an elevated density of absorbers up to 2 Mpc from galaxies. Wakker & Savage (2009) also confirmed a previously suggested correlation between Lyα absorption linewidth (W) and impact parameter ρ, observing that the broadest lines (FWHM >150 km/s) are only seen within 350 kpc of a galaxy, while at $\rho > 1$ Mpc, only lines with FWHM < 75 km/s occur.

In addition, studying the enrichment of galaxy halos is necessary for constraining outflow models and informing stellar feedback prescriptions. Directly measuring the velocity field and column densities of absorbers as a function of impact parameter and orientation around galaxies would provide the clearest evidence of inflow or outflow activity, but results are still uncertain. Kacprzak et al. (2011) claim to find that Mg II equivalent widths correlate with galaxy inclination, but Mathes et al. (2014) find no such correlation for Lyα and O VI absorbers. Furthermore, we should expect outflowing gas to be more highly enriched and trace the metallicity of the associated galaxy, with inflowing gas instead appearing only in H I. Both Stocke et al. (2013) and Liang & Chen (2014) find an "edge" to heavy ion absorption at $\sim 0.5R_{vir}$, but with Lyα covering fractions of $\sim 0.75 - 1$ continuing out to R_{vir}. However, Mathes et al. (2014) measures O VI absorption out to $\sim 3\ D_{gal}/R_{vir}$ **need Savage et al 2014 here**.

Recent results from Kacprzak et al. (2011 & 2012) suggest that absorbing systems have a preferred orientation with respect to the major and minor axes of the galaxies they are associated with. This could be evidence of inflows and outflows, or an effect of the global structure of galaxy halos, but the statistics are not yet good enough to provide consistent answers. A larger-scale study of inclination and azimuthal angles vs. absorber properties is needed in order to elucidate the distribution of absorbing systems around galaxies. This is most easily done for the largest galaxies in the nearby universe, where it is possible to obtain inclinations and unambiguous absorber associations.

Previous studies have suffered from small sample sizes (e.g. Mathes et al. 2014 use 14 galaxies, Stocke et al. 2013 use 11, Werk et al. 2014 use 44), and incompleteness due to their higher mean redshifts (e.g. the Mathes et al.

2014 sample is $0.12 < z < 0.67$, and Werk et al. 2014 are complete to $\sim L^*$ at $z \sim 0.2$). To address these shortcomings, we are conducting a large survey of the properties of intergalactic gas in the nearby universe, where we have good and relatively complete information on both faint and bright galaxies, in order to reveal how the IGM and galaxies affect each other. We are taking advantage of the over 300 archived QSO and Seyfert spectra taken by the Cosmic Origins Spectrograph (COS) and Space Telescope Imaging Spectrograph (STIS) on the Hubble Space Telescope (HST), combined with the wealth of information available for the $\sim 100,000$ galaxies with $cz < 10,000$ km/s found in the NASA Extragalactic Database (NED) to probe the environment of absorbing gas systems in the nearby universe. This approach allows for an unbiased understanding of the distribution of the gas around galaxies, which requires looking for both detections and non-detections of gas, both near as well as far away from galaxies.

This paper presents initial results from our pilot study of 35 sight lines, chosen for their proximity to large galaxies and ease of spectral feature identification. This paper is organized as follows: in Section 2 we present the data and analysis techniques, in Section 3 we present the results, and in Section 4 we discuss possible interpretations of our results.

2. DATA AND ANALYSIS

2.1. *Galaxy Data*

Each final, combined, and identified sightline is correlated with the galaxy environment in order to match absorption features with galaxies near the sightline. To facilitate this, we have constructed a dataset of all $z \leq 0.033$ ($v \leq 10,000$ skm/s) galaxies with published data available through the NASA Extragalactic Database (NED[1]). This dataset contains over 108,000 entries, and includes data from SDSS, 2MASS, 2dF, 6dF, RC3, and many other, smaller surveys. Our criteria for including a galaxy in this dataset is only an accurate, spectroscopic redshift which places the galaxy in the $400 \leq v \leq 10,000$ km/s velocity range. This restriction naturally leads to a completeness limit of $B \lesssim 18.7$ mag **CHECK THIS**, or $\sim 0.1L_*$ on average across the sky (see Figure 1). For any particular region of the sky, this limit will vary some depending upon which of the larger surveys cover the region.

In addition, we have homogenized the galaxy data beyond the steps taken by NED by normalizing all measurements of galaxy inclination, position angle, and diameter to 2MASS K-band values. Most galaxies in NED have measures of inclination, position angle and diameter available in several different bands, so in order to make meaningful comparisons, it is necessary to choose one band for all measurements. We chose 2MASS values for this because it was an all-sky survey, and represents the largest fraction of available galaxy data. Physical galaxy diameters are derived from 2MASS K_s "total" angular diameter measurements and galaxy distances. 2MASS K_s "total" diameter estimates are surface brightness extrapolation measurements and are derived as

$$r_{tot} = r' + a(ln(148)^b, \quad (1)$$

where r_{tot} is defined as the point where the surface brightness extends to 5 disk scale lengths, r' is the starting point radius ($> 5" - 10"$ beyond the nucleus, or core influence), and a and b are Sersic exponential function scale length parameters ($f = f_0 \exp(-r/a)^{(1/b)}$, see Jarret et al. 2003 for a full description). **NEEDS TO BE CHECK FOR FULL SKY** Approximately 50% of all the galaxies have this 2MASS K_s "total" diameter. Of the remainder, 20% have SDSS diameters, 27% have no published diameter, and 3% have diameters from other surveys. We convert values in these other bands to 2MASS K_s "total" diameters via a simple least squares linear fit when necessary.

We used B-band magnitudes to estimate each galaxy's luminosity as a ratio of L_* as follows:

$$\frac{L}{L_*} = 10^{-0.4(M_B - M_{B_*})}. \quad (2)$$

We adopt the CfA galaxy luminosity function by Marzke et al. (1994), which sets B_* = -19.57. Direct B band measurements are available for $\sim$ 30% of galaxies, and most of the rest have SDSS g and r magnitudes, which can be converted to B via $B = g + 0.39(g-r) + 0.21$ (Jester et al. 2005). Finally, we also compute an estimate of the virial radius of each galaxy as $logR_{vir} = 0.69logD + 1.24$. This follows the parametrization of Stocke et al. (2013) relating a galaxy's luminosity to its virial radius, and the Wakker & Savage (2009) empirical relation between diameter and luminosity (see Wakker et al. 2015 and references therein for further details).

This homogeneous galaxy data table allows us to draw direct comparisons between the properties of the absorbers and the properties, separations, and environments of nearby galaxies, with unprecedented completeness. The full dataset will be publicly released and discussed in further detail in a forthcoming paper.

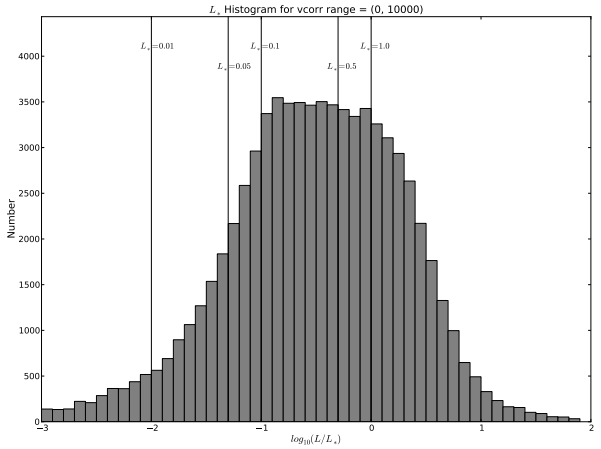

Figure 1. Distribution of L/L_* values for all galaxies in the dataset. Black vertical lines highlight 1, 0.5, 0.1, 0.05 and 0.01 L_*. The turnoff around $0.1L_*$ shows that on average, the dataset is complete to $0.1L_*$.

[1] This research has made use of the NASA/IPAC Extragalactic Database (NED) which is operated by the Jet Propulsion Laboratory, California Institute of Technology, under contract with the National Aeronautics and Space Administration.

Target	R.A.	Dec.	z	Program	PI	Obs ID	Obs Date	T_{exp} [ks
MRK290	15 35 52.3	+57 54 09	0.0296	11524	Green	LB4Q02	2009 10 28	3.9
SBS1537+577	15 38 10.0	+57 36 13	0.0734	12276	Wakker	LBI606	2011 10 19	5.2
3C66A	02 22 39.6	+43 02 08	0.4440	12612	Stocke	LBXC04	2012 11 1	26.4
3C66A	02 22 39.6	+43 02 08	0.4440	12863	Furniss	LC0J01	2012 11 8	26.4
MRC2251-178	22 54 05.9	-17 34 55	0.0661	12029	Green	LBGB03	2011 09 29	4.6
SBS1503+570	15 04 55.6	+56 49 20	0.3589	12276	Wakker	LBI617	2011 10 19	5.2
SDSSJ080838.80+051440.0	08 08 38.8	+05 14 40	0.3610	12603	Heckman	LBS330	2012 03 17	4.7
2dFGRS_S393Z082	02 45 00.8	-30 07 23	0.3400	12988	Bowen	LC1045, LC1040	2013 05 27,28,29	17.7
PG1211+143 (STIS)	12 14 17.7	+14 03 13	0.0804	8571	Shull	XXXXXX	1999 07 22, 2002 02 0,4,5,6,7,8	67.4
TON488	10 10 00.7	+30 03 21	0.2564	12025	Green	LBG810, LBG811	2011 05 19,21	10.8
SDSSJ135341.03+361948.0	13 53 41.0	+36 19 48	0.1470	13444	Wakker	LC8L04	2014 06 14	4.6
MRK1014	01 59 50.2	+00 23 41	0.1630	12569	Veilleux	LBP404	2012 01 25	1.8
RX_J1503.2+6810	15 03 16.5	+68 10 06	0.1140	12276	Wakker	LBI609	2010 12 31	1.9
PG1302-102	13 05 33.0	-10 33 20	0.2784	12038	Green	LBGL04	2011 08 16	6.0
SBS1108+560	11 11 32.1	+55 47 25	0.7650	12025	Green	LBG809	2011 05 12	8.4
PG1216+069	12 19 20.9	+06 38 38	0.3313	12025	Green	LBG881	2012 02 4,5	5.1
IRAS_Z06229-6434	06 23 07.7	-64 36 19	0.1289	11692	Howk	LB3J09, LB3J58	2009 12 19, 2010 09 15	8.7
SDSSJ080908.13+461925.6	08 09 08.1	+46 19 26	0.6563	12248	Tumlinson	LBHO77	2010 10 06	3.1
TON1009	09 09 06.1	+32 36 31	0.8090	12603	Heckman	LBS328	2012 04 22	4.7
RX_J1330.8+3119	13 30 53.2	+31 19 32	0.2410	12248	Tumlinson	LBHO85	2011 07 11	4.3
SDSSJ140428.30+335342.0	14 04 28.3	+33 53 42	0.5490	12603	Heckman	LBS320	2013 03 03	7.7
RX_J0714.5+7408	07 14 36.2	+74 08 11	0.3710	12275	Wakker	LBH402	2011 03 18	8.3
PG1121+423	11 24 39.2	+42 01 45	0.2340	12024	Green	LBG703	2011 04 25	5.0
RBS2070	23 59 07.8	-30 37 39	0.1650	12864	Fang	LC0F01	2013 06 15,19	17.0
3C351.0	17 04 41.4	+60 44 31	0.3719	8015	Jenkins	O57901	1999 06 27	77.0
HE1228+0131	12 30 50.0	+01 15 21	0.1170	11686	Arav	XXXXXX	XXXXXXX	11.0
3C273.0	12 29 06.7	+02 03 08	0.1583	12038	Green	LBGL31	2012 04 22	4.0
PG1626+554	16 27 56.2	+55 22 32	0.1330	12029	Green	LBGB01	2011 06 15	3.3
PG1307+085	13 09 47.0	+08 19 47	0.1550	12569	Veilleux	LBP411	2012 06 16	1.8
PKS2005-489	20 09 25.4	-48 49 53	0.0710	11520	Green	LB4R03	2009 09 21	2.5
CSO395	12 11 14.6	+36 57 39	0.1690	12248	Tumlinson	LBH062	2011 04 27	3.0
HS0624+6907	06 30 02.6	+69 05 03	0.3700	9184	Tripp	XXXXXX	2002 01 2, 2002 02 23,24	62.0
HE0238-1904	02 40 32.6	-18 51 51	0.6310	11541	Green	LB6804	2009 12 31	14.4
RBS1795	21 54 51.0	-44 14 05	0.3440	11541	Green	LB6809	2010 06 23,24	8.2
H1101-232	11 03 37.7	-23 29 31	0.1860	12025	Green	LBG804	2011 07 5,6	13.3
1H0717+714	07 21 53.3	+71 20 36	0.5003	12025	Green	LBG812	2011 12 27	6.0
PG0003+158	00 05 59.3	+16 09 49	0.4509	12038	Green	LBGL17	2011 10 22	10.4
SBS1122+594	11 25 53.7	+59 10 22	0.8580	11520	Green	LB4R11	2009 11 07	10.0

Table 1
Observations

2.2. *Spectra*

This initial pilot study contains 35 sightlines to bright QSOs observed with COS (34 of 35) and STIS (1 of 35). We chose sightlines by first sorting the galaxy data table described above by diameter. This sorted list is then correlated with the full list of available sightlines, and only systems with impact parameter less than 500 Mpc are kept. Finally, we reject any messy, overly complicated sightlines, or low S/N sightlines and select the top 35 (again, sorted by galaxy diameter).

We chose sight lines based on high S/N (generally >10), ease of spectral identification, and proximity to large, nearby galaxies. Several are included simply because they already have published identifications. There were no strict cutoffs for galaxy size or brightness, we simply selected the top 35 sight lines after rejecting those with lower S/N and/or more complicated features. Table 2 summarizes the properties of the QSO targets we selected. **Should this just be a single table with all absorption features, associated galaxies and QSO info combined?**

All COS spectra for the target sight lines was obtained through the Barbara A. Mikulski Archive for Space Telescopes (MAST), and processed with CALCOS v3.0. We combined individual exposures by the method of Wakker et al. (2015), which corrects the COS wavelength scale by cross-correlating all ISM and IGM lines in each exposure. This method addresses the up to ±40 km/s misalignments produced by CALCOS, and produces a corrected error array based on Poisson noise, which better matches the measured errors then the errors delivered in the x1d files. We then combine multiple exposure by aligning Galactic absorption lines with 21-cm spectra, and adding up the total counts in each pixel before converting to flux using the original, average flux-count ratio at each wavelength.

3. RESULTS

We have identified 176 Lyα absorption lines in the spectra of 35 background QSOs. Of these, 32% can be unambiguously associated with a single nearby galaxy, while 53% reside in relative voids (greater than $\rho = 500$

Target	Galaxy	$\mathcal{L}$	R_{vir} [kpc]	ρ (kpc) [kpc]	v_{galaxy} [km/s]	Δv [km/s]	Inc. [deg]	Az. [deg]	$v_{Ly\alpha}$ [km/s]	$W_{Ly\alpha}$ [mÅ]
(1)	(2)	(3)	(4)	(5)	(6)	(7)	(8)	(9)	(10)	(11)
MRK290	KKR19	1.3e-52	41	449	936	177.7	48	x	758	134±10
MRK290	NGC5987	0.87*	322	486	3170	65	65	12	3105	511±5
MRK290	NGC5987	0.94*	322	486	3170	-37	65	12	3207	319±4
SBS1537+577	UGC05470	0	11	319	534	-219.7	41	38	754	146±36
SBS1537+577	NGC5987	0.79*	322	454	3170	-109	65	33	3279	358±30
SBS1537+577	SDSSJ153802.75+573018.3	0.21	87	91	3687	138.3	80	15	3549	447±28
SBS1537+577	SDSSJ153802.75+573018.3	0.0076	87	91	3687	-389.7	80	15	4077	72±25
MRC2251-178	MCG-03-58-014	5.2e-20	64	417	1993	-264.8	56	6	2258	80±5
MRC2251-178	HIPASSJ2254-18	0.00096	122	320	2991	-51.5	53	56	3042	67±5
MRC2251-178	HIPASSJ2254-18	0.00033	122	320	2991	-212.5	53	56	3203	332±5
MRC2251-178	MCG-03-58-009	0.16*	319	320	8754	-297.2	59	39	9051	60±4
SDSSJ080838.80+051440.0	UGC04239	0.49*	279	378	8893	153.1	44	38	8740	883±24
SDSSJ080838.80+051440.0	UGC04239	0.85*	279	378	8893	-33.9	44	38	8927	130±19
SDSSJ080838.80+051440.0	2MASXJ08083956+0517256	0.0083	106	106	9371	-389	26	71	9760	58±15
2dFGRS_S393Z082	NGC1097	0.62*	273	112	1030	-209.2	47	12	1239	570±21
PG1211+143	NGC4189	0.0053	181	314	2415	298.5	55	84	2116	105±8
PG1211+143	SDSSJ121430.17+141512.6	0.00011	117	351	6930	-59.5	76	26	6989	131±6
PG1211+143	SDSSJ121352.97+141312.4	9.2e-08	91	368	7711	-24.5	50	51	7735	156±8
TON488	UGC05478	0.044	92	58	1620	370.3	12	x	1250	68±9
TON488	UGC05478	0.3	92	58	1620	245.3	12	x	1375	452±12
MRK1014	KUG0156-001	2.5e-05	141	446	5538	-156	36	12	5694	45±9
MRK1014	NGC0768	0.0087*	253	486	6752	-327.7	73	85	7080	117±11
MRK1014	SDSSJ020017.78+003715.5	1.9e-07	122	477	7638	75.2	67	59	7563	416±10
RX_J1503.2+6810	CGCG318-012	0.25*	250	325	9912	-210.2	50	1	10122	44±14
PG1302-102	MCG-02-34-006	4.1e-05	132	405	1481	167.7	34	x	1313	322±7
PG1302-102	NGC4939	0.77*	235	265	3382	-66.2	46	61	3448	71±5
PG1302-102	PKS1302-102:[CPC2008]1027	x	x	336	7829	253.3	x	x	7576	37±4
SBS1108+560	UGC06225	0.89	228	29	910	178.4	77	82	732	1082±82
SBS1108+560	UGC06225	2.0	228	29	910	-18.6	77	82	929	284±51
PG1216+069	SDSSJ121903.72+063342.9	0.0072	71	110	4131	318	61	65	3813	360±10
SDSSJ080908.13+461925.6	UGC04260	0.00018	75	218	2391	110	65	42	2281	85±12
SDSSJ080908.13+461925.6	SDSSJ080842.74+461828.9	0.013	103	133	7227	327.2	37	4	6900	151±10
SDSSJ080908.13+461925.6	SDSSJ080842.74+461828.9	0.14	103	133	7227	110.2	37	4	7117	176±12
TON1009	NGC2770	0.083*	204	274	2143	182.1	78	43	1961	350±21
TON1009	KUG0906+333ANED01	2.5e-11	101	495	3901	108.9	64	x	3792	132±12
TON1009	IC2439	0.4	153	109	4495	209.8	71	51	4285	343±17
RX_J1330.8+3119	UGC08496NED02	0.014	101	160	5104	265.2	59	46	4839	413±16
RX_J1330.8+3119	UGC08492	0.01*	204	335	7689	288.2	16	41	7401	330±15
SDSSJ140428.30+335342.0	KUG1402+341	0.17	204	118	8178	293.5	69	63	7884	889±28
RX_J0714.5+7408	UGC03739	1.2e-29	58	475	1201	-138.5	39	x	1339	24±8
RX_J0714.5+7408	UGC03717	0.069*	202	271	4269	194.8	61	83	4074	58±7
RX_J0714.5+7408	UGC03717	0.18*	202	271	4269	4.8	61	83	4264	410±9
PG1121+423	SDSSJ112418.74+420323.1	0.01	104	129	7628	349	65	20	7279	46±6
PG1121+423	SDSSJ112418.74+420323.1	0.023	104	129	7628	300	65	20	7328	359±7
3C351.0	SDSSJ170325.13+603944.4	0.00041	116	315	7328	135.7	44	24	7192	63±11
HE1228+0131	NGC4517	0.27	193	211	1420	-67.6	83	74	1488	144±3
HE1228+0131	NGC4517	0.19	193	211	1420	-135.6	83	74	1556	20±2
HE1228+0131	2MASXJ12303439+0116243	0.0063	127	159	9613	373.8	28	60	9239	249±3
3C273.0	SDSSJ122840.21+015426.8	3.9e-20	62	406	9083	250.5	28	x	8832	139±2
3C273.0	SDSSJ122830.42+020630.6	6.7e-09	99	402	10144	311.7	30	x	9832	40±2
PG1307+085	CGCG072-007	0.0036	193	440	7413	134.2	50	43	7279	64±7
H1101-232	MCG-04-26-019	0.058	173	179	3846	266.2	65	26	3580	573±12
1H0717+714	UGC03804	0.18	173	207	2973	102.8	53	7	2870	343±6
1H0717+714	UGC03804	0.24	173	207	2973	16.8	53	7	2956	39±4
PG0003+158	NGC7814	0.25	171	197	789	-43.7	65	47	833	131±15
SBS1122+594	IC0691	0.53	66	45	1399	185.4	42	56	1214	830±13

Table 2
All associated systems. The largest $\mathcal{L}$ value is given, where a (*) indicates $d^{1.5}$ was used, otherwise the quoted $\mathcal{L}$ was computed with R_{vir}. For all entries, 'x' indicates unknown values.

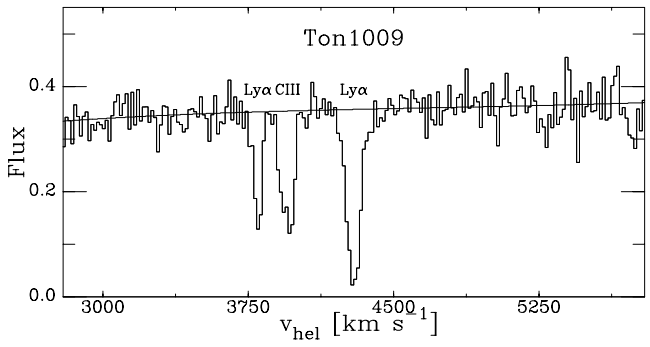

(a)

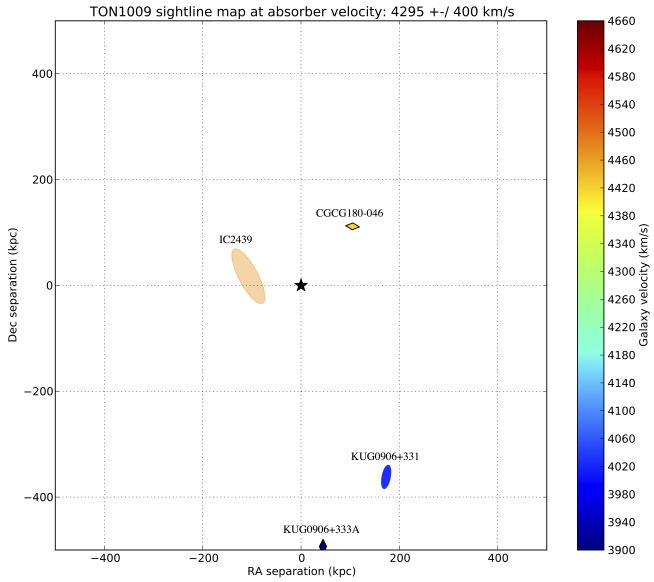

(b)

Figure 2. a) An example Lyα line found in a sightline towards target TON1009 at 4295 km/s. b) A map of *all* galaxies within a 500 kpc impact parameter target TON1009 sightline and with velocity (cz) within 400 km/s of absorption detected at 4295 km/s (central black star). The galaxy IC2439 (v = 4494 km/s, inclination = 71°) can be unambiguously paired with the Lyα absorption feature at v = 4295 km/s because it is the largest and closest galaxy in both physical and velocity space to the absorption feature.

kpc and $\Delta v = 400$ km/s from any galaxy). In order to be considered for a pairing, a galaxy and absorption feature must appear within 400 km/s in velocity and 500 kpc in physical impact parameter from each other. When multiple galaxies pass these criteria for a particular line, we are left with two options. 1) one galaxy is obviously far larger and closer in physical and velocity space to the line, and may have several satellite galaxies, or 2) no single galaxy if obviously dominant, and we do not include this line in further analysis.

To facilitate this decision, we compute the likelihood, $\mathcal{L}$, of every possible galaxy-absorber pairing as follows:

$$\mathcal{L} = Ae^{-(\frac{\rho}{R})^2} e^{-(\frac{\Delta v}{200})^2}. \quad (3)$$

Here ρ is the physical impact parameter, Δv the velocity difference between the absorber and the galaxy ($\Delta v = v_{galaxy} - v_{absorber}$), and A is a factor included to increase

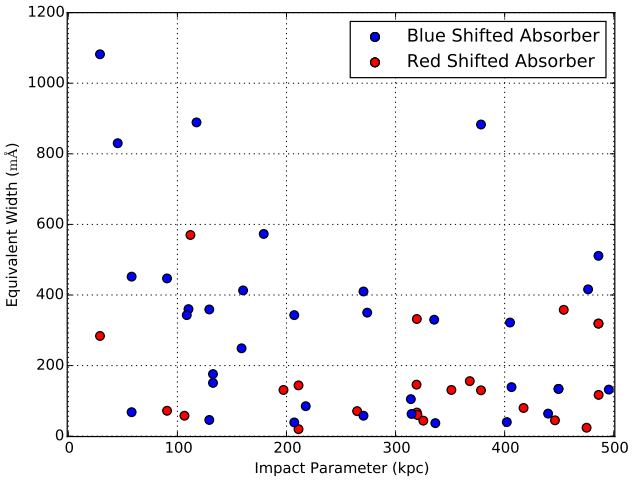

(a)

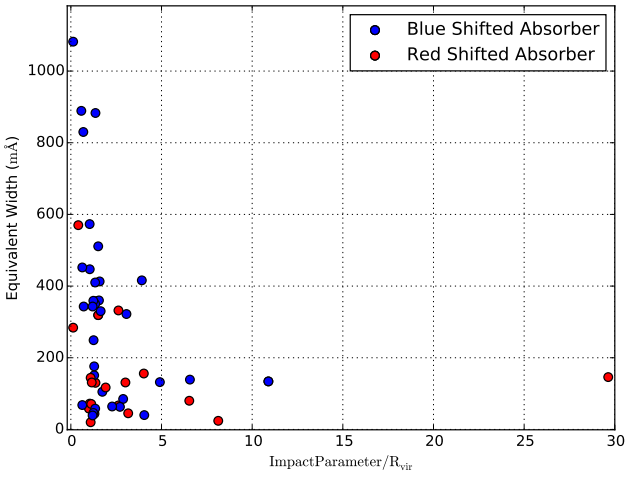

(b)

Figure 3. a) Equivalent width (W) of each absorber as a function of ρ (kpc), the physical impact parameter between the galaxy and the sightline toward the absorption feature. b) (W) as a function of ρ/R_{vir}, the ratio of the physical impact parameter and the galaxy diameter. The anti-correlation is strongest when scaling ρ by the galaxy virial radius.

the likelihood in the case that $R \geq \rho$ (in which case $A = 2$, otherwise $A = 1$). We compute $\mathcal{L}$ for two different values of R: R_{vir}, the virial radius of the galaxy, and $d^{1.5}$, the major diameter of the galaxy to the power of 1.5. $\mathcal{L}$ computed with R_{vir} is liable to select satellite galaxies instead of the larger hosts, so including a version with $d^{1.5}$ serves as a two-tiered selection system. An absorber-galaxy system separated by 200 km/s in velocity and $1R_{vir}$ would have $\mathcal{L} = 0.27$. In order for an absorber to be marked as "associated" with a particular galaxy, its $\mathcal{L}$ must be a factor of 5 larger than the next best possible association. We visually inspect each system before it is included in the final sample.

Figures 2.1 and 2(b) show a clean example of a Lyα absorption line with a map of its galaxy environment, showing an unambiguous pairing between the absorption feature at 4295 km/s toward TON1009 and galaxy IC2439

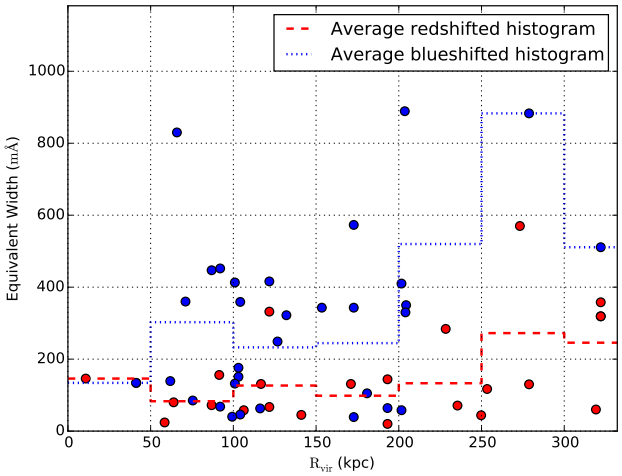

Figure 4. Equivalent width (W) of each absorber as a function of the virial radius of the associated galaxy in the sample. The blue-dotted and red-dashed lines shows the average W in 50 kpc bins of R_{vir} for the blueshifted and redshifted absorbers, respectively.

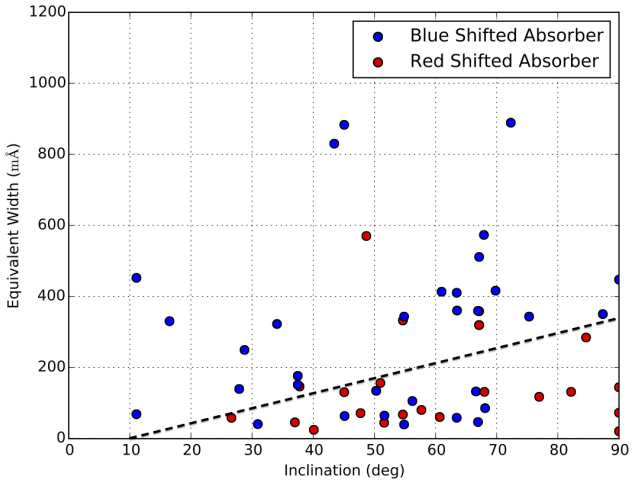

Figure 5. Equivalent width (W) of each absorber as a function of the inclination angle of the associated galaxy in the pilot study sample. The dashed black line is drawn to highlight the separation between red and blue shifted absorption systems (with respect to the systemic velocity of the galaxy).

($\mathcal{L} = 0.45$). Unless explicitly stated, all following analysis concerns similarly unambiguous "associated" systems.

Most interestingly, new results emerge when we split the absorber-galaxy catalog based on the velocity difference of the two. We define the differential velocity between the absorption and an associated galaxy as follows:

$$\Delta v = v_{galaxy} - v_{absorber}. \tag{4}$$

With this scheme, we refer to an absorber with a velocity *lower* than the associated galaxy as *blueshifted*, while an absorber with a velocity *higher* is referred to as *redshifted*. The rest of the results will be analyzed based upon this splitting. For all distributions, we employ and quote the results of both the Kolmogorov-Smirnov (KS) and the Anderson-Darling (AD) statistical tests.

3.1. *W-ρ Anti-correlation*

As mentioned earlier, numerous previous studies have found that Lyα equivalent width (W) is anti-correlated with impact parameter (ρ) to the nearest galaxy. We find a weak correlation, as shown in Figure 3(a). However, we find a much stronger anti-correlation when we normalize ρ by R_{vir}. Figure 3(b) shows this expected anti-correlation when plotting W vs ρ/R_{vir}. The obvious explanation for this is that larger galaxies host larger, more physically extent CGM halos. We would thus expect W to also correlate positively with R_{vir}. Figure 4 shows W as a function of R_{vir}, with the blue-dotted and red-dashed lines show the average W in bins of 50 kpc of R_{vir}. A slight, positive correlation is evident between equivalent width and galaxy virial radius.

3.2. *Inclination*

In this section we examine the inclinations of the associated galaxies compared to the red and blueshifted distributions of absorbers. We compute galaxy inclination, i, as follows:

$$\cos(i) = \sqrt{\frac{q^2 - q_0^2}{1 - q_0^2}}, \tag{5}$$

where $q = b/a$, the ratio of the minor to major axis, and q_0 is the intrinsic axis ratio, set to $q_0 = 0.2$ for all galaxies.

Figure 5 shows red and blueshifted absorbers' W plotted against the inclinations of their associated galaxies. We note that there is a clear dichotomy between the distributions, where blue shifted absorbers appear around nearly all inclinations of galaxies, but redshifted absorbers appear preferentially near highly-inclined galaxies ($i \geq 50$ deg). In addition, redshifted absorbers appear with lower W than those blueshifted across all inclinations. The average W of all redshifted absorbers is $\langle W \rangle = 153 \pm 14$ mÅ, compared to $\langle W \rangle = 321 \pm 13$ mÅ for blueshifted absorbers. We can reject the null hypothesis that red and blue shifted absorbers come from the same underlying distribution at the 98% level (results of both KS and AD tests).

In total, 64% of blueshifted and 68% of redshifted absorbers are associated with high inclined galaxies ($i \geq 50$ deg). 56% of all galaxies in the survey volume are highly inclined, indicating a slight preference for detecting absorption around inclined galaxies. However, KS and AD tests do not assign high significance to this result.

3.3. *Azimuth*

In this section we examine properties of absorbers as a function of their azimuthal angle with respect to their associated galaxy. Azimuth is defined as the angle between the major axis of a galaxy and the vector connecting the absorption feature and the midpoint of the galaxy plane. Figure 6 illustrates this. The mean azimuth angle for blueshifted absorbers is 41°, and 42° for redshifted absorbers. Figure 7 shows the distribution of azimuth angles for both red and blue-shifted absorbers. Contrary

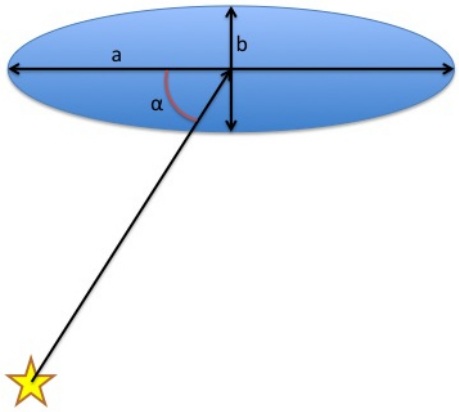

Figure 6. Azimuth is the angle, α, between the major axis of the galaxy, a, and a vector extending from the AGN target to the galaxy center.

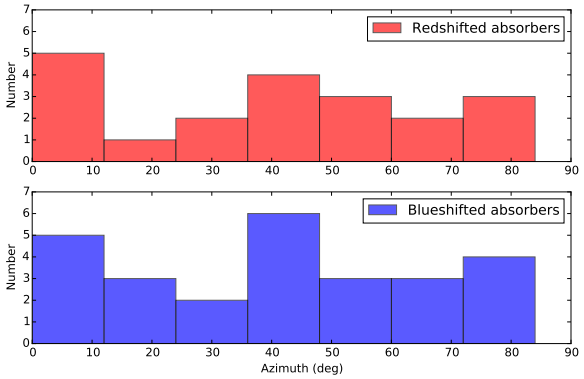

Figure 7. The distributions of azimuth angles for redshifted systems (top, red), and blueshifted systems (bottom, blue).

to the findings of Kacprzak et al. (2011, 2012), who claim to find a bimodal distribution of Mg II absorbers around galaxies, our distributions of Lyα absorbers are consistent with a flat, random distribution. There is a slight overabundance of absorbers around 45% azimuth in both samples, but we cannot assign this observation much significance given the small sample size. We additionally find no significant correlation between azimuth angle and W or Δv.

4. DISCUSSION

Why would there be a preference for gas blue-ward of galaxies, or equivalently, gas falling onto a galaxy from behind? If the gas is co-rotating, then this would mean that most absorbers we detect are on the side of the galaxy moving toward us, and that they tend to be higher equivalent width clouds.

WHAT'S THE MEAN L_* OF ASSOCIATED GALAXIES? AND ALL THE FIELDS IN GENERAL?

5. SUMMARY

We have measured 175 Lyα absorption lines in the spectra of 33 COS and 2 STIS targets. Using a new likelihood parameter, we have match 56 of these lines with nearby galaxies. The following summarizes our findings:

- W anti-correlates most strongly with ρ when normalized by R_{vir}. It follows that W weakly correlates and anti-correlates with R_{vir} and ρ, respectively.
- We find a dichotomy in the W of absorption blue-ward vs red-ward of associated galaxies. Redshifted absorbers are far weaker, with $W = 153 \pm 14$ mÅ compared to $W = 321 \pm 13$ mÅ for blueshifted absorbers. KS and AD test show at greater than 98% (KS = 98%, AD = 99%) confidence level that these two sets of absorbers are drawn from different distributions.
- Lyα absorbers are most associated with inclined galaxies. 64% of blueshifted and 68% of redshifted absorbers are associated with galaxies with $i \geq 50$ deg, whereas 56% of all galaxies in the survey volume have similarly high inclinations.